STRUCTURAL STABILITY AND BIFURCATION FOR 2-D INCOMPRESSIBLE FLOWS WITH SYMMETRY*

CHUN-HSIUNG HSIA†, JIAN-GUO LIU‡, AND CHENG WANG§

Abstract. This article studies the structure and its evolution of incompressible flows with the anti-symmetry using a combination of rigorous analysis and numerical simulations, with an application to an example of oceanic flow. In particular, necessary and sufficient conditions for 2D divergence-free vector fields with anti-symmetry are obtained, and a detailed numerical simulation for a simplified model of Marsigli oceanic flow is provided to explore and verify the structure and its transitions of the flow. It is expected that the study will lead to useful insights to the understanding of the flow dynamics from both the mathematical and physical points of view.

Key words. Divergence-free velocity vector, structural stability and bifurcation, symmetric stability, saddle connection.

AMS subject classifications. 35Q30, 35Q35, 65M06, 76D05

1. Introduction. As we know, if the symmetry is enforced in the flow past a circular cylinder, some unstable nature such as the famous von Kármán street will not appear. The enforcement of the symmetry sometimes can be used to idealize the flow to study some local flow behavior such as boundary layer separation. A symmetric flow appears in many situations. For example, it may come from the symmetry of domain, force, etc. The main objectives of this article are two-fold. First, we prove a structural stability result for divergence-free vector fields with central symmetry. Then we numerically examine stability and transitions of the flow structure in the physical space for the 2-D Boussinesq flows with central symmetry.

In this paper, we study the structure and its transitions of two-dimensional incompressible flows with symmetry. This is part of a research program recently initiated by T. Ma and S. Wang to develop a geometric theory of two-dimensional (2-D) incompressible fluid flows in the physical spaces. This program of study consists of research in directions: 1) the study of the structure and its transitions/evolutions of divergence-free vector fields, and 2) the study of the structure and its transitions of velocity fields for 2-D incompressible fluid flows governed by the Navier-Stokes equations or the Euler equations.

The first important issue is the structural stability, as it has been the main driving force behind much of the development of dynamical systems theory; see among many others [1, 2, 4, 5, 6, 14, 15, 16, 18], for a detailed discussion. The necessary and sufficient conditions for structural stability of a divergence-free vector field was given by Ma and Wang in [11]. It is proven that u is structurally stable under divergence-free vector field perturbations if and only if: (1) u is regular, (2) all interior saddle points of u are self-connected, and (3) each saddle point of u on ∂M is connected to a saddle point on the same connected component of ∂M.

*Received November 14, 2008; accepted for publication November 27, 2008.

†Department of Mathematics, National Taiwan University, No. 1, Sec. 4, Roosevelt Rd., Taipei City 10617, Taiwan (willhsia@math.ntu.edu.tw).

‡Department of Physics and Department of Mathematics, Duke University, Durham, NC 27708, USA (jliu@phy.duke.edu).

§Department of Mathematics, University of Massachusetts Dartmouth, North dartmouth, MA 02747-2300, USA (cwang1@umassd.edu).

This result gives an indication on the study of structural bifurcation for 2-D incompressible fluid with no-penetration, no-slip boundary condition. If one of the three conditions is violated, the velocity vector field turns unstable. Thus, the possibility of structural transition occurs. In particular, the velocity field u turns structurally unstable if a connection occurs between two saddle points. Such an instability is proven by a saddle-breaking technique, which shows that any small perturbation near a saddle point can lead to the break-down of the saddle connection. The detail of saddle-breaking is given in T. Ma and S. Wang [11]. However, for a divergence-free vector field u with anti-symmetry with respect to a point O, i.e., the velocity field satisfies $u(O - x) = -u(x)$, a connection between symmetric saddles is stable. In other words, the structure of saddle connections between symmetric saddles remains stable under symmetric perturbations. More precisely, with the notation $R^r(TM) = \{u \in D^r(TM) | \quad u(-x, -y) = -u(x, y)\}$, it is proven in Theorem 2.5 below that u is structurally stable in $R^r(TM)$ if and only if (1) u is regular, (2) any interior saddle point P of u is either self-connected or connected to its symmetric image $P' = -P$, and (3) each boundary saddle point of u is connected to another saddle point on the same connected component of ∂M or to its symmetric image. This theorem indicates more structurally stable flow patterns under perturbation of anti-symmetric divergence-free fields.

Such an additional stability is also demonstrated by a numerical example of a Boussinesq flow induced by a temperature jump in an insulated box $[0, 8] \times [0, 1]$. This example is a simplified version of Marsigli flow which has been known since the 17th century. See [7] for a detailed description. The initial temperature is set to be 1.025 at the left half and 0.975 at the right half. Since the initial partition is located at the middle $x = 4$, the flow keeps symmetry with respect to the center point $O(4, \frac{1}{2})$. This flow is computed by a fourth order finite difference method proposed in [9], using the resolutions 2049×257 and 4097×513. To understand the flow structures and their transition, we look at the phase diagrams in a sequence of time. The computational result shows that the symmetric divergence-free velocity field keeps stable if an interior saddle is connected to its symmetric image. Meanwhile, an instability is observed if a connection between non-symmetric saddle points occurs. This provides a strong numerical evidence of the stability criterion given above.

In addition, interior structural bifurcation and separation caused by an appearance of a degenerate singular point (which violates the first condition in the stability classification theorem) plays an important role in the evolution of the flow. Spin off or disappearance of a bubble (center) represents a physical explanation of the corresponding structural transition. Some relevant discussions of pattern formation and transition for incompressible fluid can be found in earlier literatures [3, 8, 17]. A theoretical analysis of such a bifurcation was recently given by T. Ma and S. Wang [12]. It is proven that an interior transition of topological structure occurs if the divergence-free velocity field has an isolated interior degenerate singular point with zero index and non-zero Jacobian matrix, and with non-zero acceleration in the direction normal to the eigen-space of the Jacobian. In particular, the zero index of the singular point for the velocity corresponds to the case that the angle between the two orbits connected to the critical point is zero.

All the kinematic conditions in the structural bifurcation classification theory can be verified by numerical calculation in a convenient way. For the Boussinesq flow computed in our numerical example, there are 10 structural transitions from the beginning to $t = 18.973$. Eight of them are caused by an appearance of a degenerate

singular point and the other two are caused by saddle connections between non-symmetric ones. The process and mechanism of each bifurcation are presented in detail. At each bifurcation, we see that the topological structures of the flow are stable before and after the critical time, and the only instability occurs at the critical time.

This article is organized as follows. The stability classification theory and its proof are given in Section 2. In Section 3 we recall a theorem for the interior structural bifurcation. Section 4 presents the numerical example of the Boussinesq flow. The symmetric stability is clearly illustrated and the detail of the structural bifurcation is shown.

2. Structural stability of divergence-free vector fields with symmetry. We first recapture a geometric theory for the structural analysis of 2-D divergence-free vector field with the Dirichlet boundary condition; see [13].

Let $M \subset \mathbb{R}^2$ be a closed and bounded domain with $C^{r+1}(r \geq 2)$ boundary ∂M, and TM be the tangent bundle of M. Denote

$$\begin{aligned} C_n^r(TM) &= \{u \in C^r(TM) | \quad u_n|_{\partial M} = 0\}, \\ D^r(TM) &= \{u \in C^r(TM) | \quad u_n|_{\partial M} = 0, \text{div } u = 0\}, \\ B_0^r(TM) &= \{u \in D^r(TM) | \quad u|_{\partial M} = 0\}. \end{aligned}$$

Here $u_n = u \cdot n$ and $u_\tau = u \cdot \tau$, while n and τ are the unit normal and tangent vectors on ∂M respectively. By the above definition,

$$B_0^r(TM) \subset D^r(TM) \subset C_n^r(TM) \subset C^r(TM).$$

We start with some basic concepts. Let $X = D^r(TM)$ or $B_0^r(TM)$ in the following definitions.

DEFINITION 2.1. *Two vector fields u, $v \in D^r(TM)$ are called topologically equivalent if there exists a homeomorphism of $\varphi : M \to M$, which takes the orbits of u to orbits of v and preserves their orientation.*

DEFINITION 2.2. *A vector field $v \in X$ is called structurally stable in X if there exists a neighborhood $\mathcal{O} \subset X$ of v such that for any $u \in \mathcal{O}$, u and v are topologically equivalent.*

A few important facts and definitions about divergence-free vector fields are summarized as follows. See [13] for details. Let $v \in D^r(TM)$.

1. A point $p \in M$ is called a singular point of v if $v(p) = 0$; a singular point p of v is called non-degenerate if the Jacobian matrix $Dv(p)$ is invertible; v is called regular if all singular points of v are non-degenerate.
2. An interior non-degenerate singular point of v can be either a center or a saddle, and a non-degenerate boundary singularity must be a saddle.
3. Saddles of v must be connected to saddles. An interior saddle $p \in M$ is called *self-connected* if p is connected only to itself, i.e. p occurs in a graph whose topological form is that of the number 8.
4. v is structurally stable near each non-degenerate singular point of v.
5. If $v \in D^r(TM)(r \geq 1)$ be regular, then the topological set of orbits of v consists of finite connected components of circle cells, circle bands, and saddle connections.

For $u \in B_0^r(TM)(r \geq 2)$, different singularity concepts are introduced in [10]. We recall it as follows.

(a) A point $p \in \partial M$ is called a ∂-regular point of u if $\partial u_\tau(p)/\partial n \neq 0$; otherwise, $p \in \partial M$ is called a ∂-singular point of u.

(b) A ∂-singular point $p \in \partial M$ of u is called non-degenerate if

$$\det \begin{pmatrix} \frac{\partial^2 u_\tau(p)}{\partial \tau \partial n} & \frac{\partial^2 u_\tau(p)}{\partial n^2} \\ \frac{\partial^2 u_n(p)}{\partial \tau \partial n} & \frac{\partial^2 u_n(p)}{\partial n^2} \end{pmatrix} \neq 0.$$

A non-degenerate ∂-singular point of u is also called a ∂-saddle point of u.

(c) A vector $u \in B_0^r(TM)$ $(r \geq 2)$ is called D-regular if u is regular in $\overset{\circ}{M}$, and all ∂-singular points of u on ∂M are non-degenerate.

The following theorems were proved by T. Ma and S. Wang in [10, 11], providing necessary and sufficient conditions for structural stability of a divergence-free vector field.

THEOREM 2.3. ([11]) *Let $v \in D^r(TM)(r \geq 2)$. Then v is structurally stable in $D^r(TM)$ if and only if*

i) v is regular;

ii) all interior saddle points of v are self-connected; and

iii) each boundary saddle point of v is connected to a boundary saddle on the same connected component of the boundary.

Moreover, all structurally stable vector fields in $D^r(TM)$ form an open and dense set of $D^r(TM)$.

THEOREM 2.4. ([10]) *Let $u \in B_0^r(TM)(r \geq 2)$. Then u is structurally stable in $B_0^r(TM)$ if and only if*

i) u is D-regular;

ii) all interior saddle points of u are self-connected; and

iii) each ∂-saddle point of u on ∂M is connected to a ∂-saddle point on the same connected component of ∂M.

Moreover, the set of all structurally stable vector fields is open and dense in $B_0^r(TM)$.

In this article we provide the structural stability analysis for a 2-D divergence-free vector field u with anti-symmetry with respect to the origin point $O(0,0)$. i.e., the vector field $u(x,y)$ satisfies

$$u(-x,-y) = -u(x,y). \tag{2.1}$$

We denote

$$R^r(TM) = \{u \in D^r(TM) | \quad u(-x,-y) = -u(x,y)\},$$
$$S_0^r(TM) = \{u \in B_0^r(TM) | \quad u(-x,-y) = -u(x,y)\}.$$

In what follows, we say that P' is the symmetric image of a point P if $P' = -P$. Similarly, the symmetric image of a set N is represented as $N' = \{-P | P \in N\}$. Now we are in a position to state the necessary and sufficient conditions for structural stability of a divergence-free vector field with anti-symmetry.

THEOREM 2.5. *Let $u \in R^r(TM)(r \geq 2)$. Then u is structurally stable in $R^r(TM)$ if and only if*

1) u is regular;
2) any interior saddle point P of u is either self-connected or connected to its symmetric image P'; and
3) each boundary saddle point P (with symmetric image P') $\in N \subset M$, N being a connected component of ∂M with symmetric image $N' \subset M$, is connected to a boundary saddle $Q \in N \cup N' \setminus \{P, P'\}$.

Moreover, the set of all structurally stable vector fields is open and dense in $R^r(TM)$.

THEOREM 2.6. *Let $u \in S_0^r(TM)(r \geq 2)$. Then u is structurally stable in $S_0^r(TM)$ if and only if*

1) u is D-regular;
2) any interior saddle point P of u is either self-connected or connected to its symmetric image P'; and
3) each ∂-saddle point P (with symmetric image P') $\in N \subset M$, N being a connected component of ∂M with symmetric image $N' \subset M$, is connected to a ∂-saddle $Q \in N \cup N' \setminus \{P, P'\}$.

Moreover, the set of all structurally stable vector fields is open and dense in $S_0^r(TM)$.

Note that the stability conditions imply that if the symmetric center point O is in the interior of M, it must be a center or saddle. If it is a saddle, it must be self-connected. Compared to Theorem 2.4, Theorem 2.6 says that a connection between two symmetric saddle points is stable under anti-symmetric perturbations. In Section 4, this stable structure is well demonstrated in our numerical experiment. We denote

$$
\begin{aligned}
D_0^r(TM) &= \{u \in B_0^r(TM) | \quad u \text{ is regular}\}, \\
D_1^r(TM) &= \{u \in D^r(TM) | \quad u \text{ satisfies all the conditions in Theorem 2.3}\}, \\
R_1^r(TM) &= \{u \in R^r(TM) | \quad u \text{ is regular}\}, \\
R_2^r(TM) &= \{u \in R^r(TM) | \quad u \text{ satisfies all the conditions in Theorem 2.5}\}, \\
S_1^r(TM) &= \{u \in S_0^r(TM) | \quad u \text{ is } D\text{-regular}\}, \\
S_2^r(TM) &= \{u \in S_1^r(TM) | \quad u \text{ satisfies all the conditions in Theorem 2.6}\}.
\end{aligned}
$$

The proof of Theorem 2.6 is similar to that of Theorem 2.5. We sketch the proof of Theorem 2.5 as follows.

LEMMA 2.7. *$R_2^r(TM)$ is dense in $R_1^r(TM)$.*

Proof. Let $v \in R_1^r(TM) \backslash R_2^r(TM)$. Then there exist saddle connections of v which violate conditions 2) or 3) in Theorem 2.5. By saddle-breaking technique introduced in [11], we can break all such connections by a small perturbation (as small as we like). This implies that $R_2^r(TM)$ is dense in $R_1^r(TM)$. □

LEMMA 2.8. *$R_1^r(TM)$ is open and dense in $R^r(TM)$.*

Proof. As shown by Robinson in [19] , the openness and the density part of $R_1^r(TM)$ in $R^r(TM)$ can be achieved by using local Hamiltonian. □

LEMMA 2.9. *$R_2^r(TM)$ is open and dense in $R^r(TM)$.*

Density is a direct result from Lemmas 2.7 and 2.8. Henceforth, we only need to show the openness. To achieve the goal, we need the following lemma.

LEMMA 2.10. *For any $v \in R_2^r(TM)$, there exists an open neighborhood $\mathcal{O}$ of v in $R^r(TM)$ such that $\mathcal{O} \subset R_2^r(TM)$.*

Proof. We proceed the proof in the following steps.

Step 1. Since v is regular, by Lemma 2.8, we can choose $\mathcal{O}$ small enough such that $\mathcal{O} \subset R_1^r(TM)$. Thanks to structural classification theorem (see [11, 13]), the (global) structure of each $u \in \mathcal{O}$ consists of circle cells, circle bands and saddle connections.

Furthermore, the assumption of v being regular indicates that there are only a finite number of of saddles. We denote them by $\{P_i, P_i' \mid i = 1, ...m\}$, where $P_i' = -P_i$ (the symmetric image of P_i) and P_i is either an interior saddle or a boundary saddle point. By the implicit function theorem, there exists $\epsilon > 0$ such that

(2.2a) $\{B(P_i, \epsilon), B(P_i', \epsilon) \mid i = 1, ..., m\}$ are disjoint balls centered at the saddle points with radius ϵ ;

(2.2b) the neighborhood $\mathcal{O}$ of v can be chosen sufficiently small such that each $u \in \mathcal{O}$ has the same number of saddles as v does, and each $B(P_i, \epsilon)$ (or $B(P_i', \epsilon)$) contains exactly one saddle of u; and

(2.2c) if P_i is a boundary saddle of v, then the saddle point in $B(P_i, \epsilon)$ (or $B(P_i', \epsilon)$) of each $u \in \mathcal{O}$ is also a boundary saddle of u .

Step 2. Next we prove that $\mathcal{O} \subset R_2^r(TM)$ provided that $\mathcal{O}$ is sufficiently small.

Suppose the contrary, there exists a sequence $v^n \in R_1^r(TM)$ satisfying the following

(2.3a) $$v^n \to v \quad \text{as } n \to \infty ;$$

(2.3b) the saddles of v^n are $\{P_i^n, P_i^{n'} \mid i = 1, ..., m, P_i^{n'} = -P_i^n\}$ such that $P_i^n \in B(P_i, \epsilon)$ and $P_i^{n'} \in B(P_i', \epsilon), i = 1, ..., m$; and

(2.3c) without loss of generality, P_1^n is connected by an orbit of v^n to P_2^n , but P_1 is not connected by an orbit of v to P_2 .

Let $\mathcal{L}^n$ be the saddle connection between P_1^n and P_2^n of v^n, including the saddle points. Hence $\mathcal{L}^n$ is a closed segment in M. It is also obvious that $P_i^n \to P_i$ as $n \to \infty$, for $i = 1, 2$. Without loss of generality, we assume that $\mathcal{L}^n$ is the unstable manifold of P_1^n, the stable manifold of P_2^n. Then $\mathcal{L}^n$ is a complete orbit of $X^n(t)$ of v^n satisfying

(2.4) $$\frac{dX^n}{dt} = v^n\Big(X^n(t)\Big), \quad X^n(t) \to P_1^n , \quad \text{as } t \to -\infty , \qquad X^n(t) \to P_2^n , \quad \text{as } t \to +\infty .$$

If we define

$$X^n(+\infty) = P_2^n , \quad X^n(-\infty) = P_1^n ,$$

then the closed segment $\mathcal{L}^n$ is parameterized by $\{X^n(t) \mid t \in [-\infty, +\infty]\}$.

Moreover, we can re-parametrize $X^n(t)$ by arc length

$$S(t) = \int_{-\infty}^{t} |(X^n)'(t_1)|\, dt_1 = \int_{-\infty}^{t} \left| v^n\Big(X^n(t_1)\Big) \right| dt_1 .$$

As a result,

$$\frac{dX^n}{ds} = \frac{dX^n}{dt} \cdot \frac{dt}{ds} = \frac{v^n(X^n(t(s)))}{|v^n(X^n(t(s)))|} .$$

If we define $X^n(s) = X^n(t(s))$, then we have

$$\left| X^n(s_2) - X^n(s_1) \right| \le \int_{s_1}^{s_2} \left| \frac{v^n(X^n(t(s)))}{v^n(X^n(t(s)))} \right| ds = s_2 - s_1 . \tag{2.5}$$

Let $\mathrm{arc}(\mathcal{L}^n)$ be the arc length of $\mathcal{L}^n$. We note that the arc lengths $\mathrm{arc}(\mathcal{L}^n)$ have to be uniformly bounded. Namely, there exists $M > 0$ such that

$$\mathrm{arc}(\mathcal{L}^n) \le M , \qquad \text{for any} \quad n .$$

Otherwise, for each natural number m, there exists a subsequence of $\mathcal{L}^n$ converging to a trajectory of length at least m, starting from P_1 in vector field v. This violates the fact that the trajectory starting from P_1 in vector field v has a fixed arc length.

For the sake of consistency, we define

$$X^n(s) = \begin{cases} X^n(s) , & \text{if } s \le \mathrm{arc}(\mathcal{L}^n) , \\ P_2^n , & \text{if } \mathrm{arc}(\mathcal{L}^n) \le s \le M . \end{cases}$$

Since $|P_1^n - P_1| < \epsilon$, $|X^n(s_1) - X^n(s_2)| \le s_2 - s_1$, we have $|X^n(s)| < |P_1| + \epsilon + s \le |P_1| + \epsilon + M$. Hence $\{X^n(s)\}$ is uniformly bounded and equi-continuous. By Arzela-Ascoli theorem, there exists a subsequence of $\{X^n(s)\}$ which converges uniformly on $[0, M]$ and solves

$$\frac{dX}{ds} = \frac{v(X(s))}{|v(X(s))|} ,$$

a trajectory of v connecting P_1 and P_2.

This contradicts to the assumption that P_1 is not connected to P_2. This proves that when n is large, vector fields v^n and v enjoy the same saddle connection structure. This completes the proof. □

Proof of Theorem 2.5. Theorem 2.5 is a direct result of Lemma 2.9. Namely, the density part shows the necessity and the openness part implies the sufficiency. □

3. Recapitulation of interior structural bifurcation. Compared to Theorem 2.4, Theorem 2.6 explores an additional stable structure of anti-symmetric vector fields. It gives an indication on the study of structural bifurcation for a family of divergence-free vector fields with anti-symmetry. If one of the three conditions in Theorem 2.6 is violated, the velocity vector field turns unstable, thus the possibility of structural transition occurs. In this section, we recall the classification theory of

interior structural bifurcation, which was recently developed by T. Ma and S. Wang in [12]. Such a bifurcation occurs when the first condition in Theorem 2.6 is violated. i.e., an interior degenerate singular point for the velocity field u appears. It is shown that a structural bifurcation is assured under Assumption (H) given by (3.4).

Consider a degenerate singular point $x_0 \in \overset{\circ}{M}$ ($\overset{\circ}{M}$ denotes the collection of the interior points of M) for u, i.e., $u(x_0) = 0$, $\det(Du)(x_0) = 0$. In addition, we assume that $Du(x_0) \neq 0$. Since $Du(x_0)$ is singular and $Du(x_0) \neq 0$, there is a unique eigen direction of $Du(x_0)$ corresponding to the zero eigenvalue. Let e_1 be the unit eigenvector, and e_2 the unit vector orthogonal to e_1. Taking the divergence-free condition of u into account, a careful analysis shows that

$$Du(x_0)\, e_1 = 0\,, \quad Du(x_0)\, e_2 = \alpha e_1\,. \tag{3.1}$$

To characterize singular points of a vector field in more detail, we need to introduce the concept of indices. Let $p \in M$ be an isolated singular point of $v \in C_n^r(TM)$, then

$$\mathrm{ind}(v, p) = \deg(v, p), \tag{3.2}$$

where $\deg(v, p)$ is the Brouwer degree of v at p. Moreover, it is shown that

$$\mathrm{ind}(v, p) = 1 - \frac{n}{2}\,, \tag{3.3}$$

in which n refers to the number of orbits connected to the singular point p.

A characterization analysis given by T. Ma and S. Wang [12] states that any isolated degenerate singular point $x_0 \in \overset{\circ}{M}$ of $u \in D^r(TM)(r \geq 1)$ with non-zero Jacobian matrix must have index 1, -1 or 0, which corresponds to one of the three following cases:

(1) a degenerate center ($\mathrm{ind}(u, x_0) = 1$),

(2) a degenerate saddle such that the 4 orbits connected to x_0 are tangent to each other at x_0, and

(3) a point with $\mathrm{ind}(u, x_0) = 0$ such that the angle between the two orbits connected to x_0 is zero.

The third case is the only case related to the interior structural bifurcation. See the assumption below.

Assumption (H). Let x_0 be an isolated degenerate singular point of u satisfying

$$\begin{cases} u(x_0) = 0\,, \quad \det(Du)(x_0) = 0\,, \quad Du(x_0) \neq 0\,, \\ \mathrm{ind}(u, x_0) = 0\,, \quad \text{such that the angle between the two orbits} \\ \qquad\qquad\qquad\quad \text{connected to } x_0 \text{ is zero}\,, \\ \partial_t u(x_0) \cdot e_2 \neq 0\,. \end{cases} \tag{3.4}$$

The following theorem provides a theoretical justification of the structural bifurcation classification.

THEOREM 3.1. ([12])

Let $u \in C^1([0, T], B_0^r(TM))$ ($r \geq 1$) satisfy Assumption (H). Then

(1) the vector field u has a bifurcation in its local structure at (x_0, t_0). More precisely, $u(x, t)$ has no singular point in a small neighborhood of of x_0 for any $t < t_0$

(or $t > t_0$) sufficiently close to t_0, and $u(x,t)$ bifurcates at least two singular points from x_0 as $t > t_0$ (or $t < t_0$), and

(2) if $x_0 \in \overset{\circ}{M}$ is a unique singular point with index zero of u^0, then $u(x,t)$ has a bifurcation in its global structure at $t = t_0$.

The above theorem deals with structural bifurcations due to the degeneracy of singular points. Section 4 explores this point more by our numerical experiment.

4. Numerical result of symmetric stability. In this section we consider a strong shear flow induced by a temperature jump and investigate the stability and bifurcation of the flow's topological structure. This example represents a simple setup of Marsigli flow which has been known since the 17th century. To explain the setting of our numerical experiment, we refer the story described in Gill's book "Atmosphere-Ocean Dynamics" [7] as follow.

> It seems that when Marsigli went to Constantinople in 1679 he was told about a well-known undercurrent in the Bosporus: "... for the fisherman of the towns on the Bosporus say that the whole stream does not flow in the direction of Byzantium, but while the upper current which we can see plainly does flow in this direction, the deep water of the abyss, as it is called, moves in a direction exactly opposite to that of the upper current and so flows continuously against the current which is seen". That is, the undercurrent water flows toward the Black Sea from the Mediterranean. Marsigli reasoned that the effect was due to density differences: water from the Black Sea is lighter than water from the Mediterranean. The lower density of the Black Sea can be attributed to lower salinity resulting from river runoff. He then performed a laboratory experiment: A container is initially divided in two by a partition. The left side contained water taken from the undercurrent in the Bosporus, while the right side contained dyed water having the density of surface water in the Black Sea. The experiment was to put two holes in the partition to observe the resulting flow. The flow through the lower hole was in the direction of the undercurrent in the Bosporus, while the flow through the upper hole was in the direction of the surface flow.

Such a flow is governed by the 2-D incompressible Boussinesq equations

$$\begin{cases} \partial_t u + (u\cdot\nabla)u + \nabla p = \dfrac{1}{Re}\Delta u + Ri\cdot\theta\cdot\begin{pmatrix} 0 \\ 1 \end{pmatrix}, \\ \partial_t \theta + (u\cdot\nabla)\theta = \dfrac{1}{Re\cdot Pr}\Delta\theta, \\ \nabla\cdot u = 0, \end{cases} \tag{4.1}$$

where u is the velocity, p the pressure, θ the temperature, and Re the Reynolds number. Pr is the Prandtl number, the ratio of the kinematic viscosity to the heat conductivity. The Richardson number Ri accounts for the gravitational force and the thermal expansion of the fluid. One may introduce other physically relevant dimensionless quantities, such as the Rayleigh number $Ra = Ri\cdot Re^2\cdot Pr$, and the Grashof number $Gr = Ra/Pr = Ri\cdot Re^2$. For brevity of presentation we denote $\nu = 1/Re$ and $\kappa = 1/(Re\cdot Pr)$. The no-penetration, no-slip condition

$$u|_{\partial\Omega} = 0, \tag{4.2}$$

is imposed for the velocity field u, while the no-flux boundary condition

$$\frac{\partial \theta}{\partial n}\Big|_{\partial\Omega} = 0\,, \tag{4.3}$$

is imposed for the temperature field.

For simplicity, a Boussinesq flow with two initially piecewise constant temperatures in an insulated box $\Omega = [0,8]\times[0,1]$ is taken into consideration. The partition is located at $x = 4$. As a result, the flow keeps anti-symmetry with respect to the center point $O(4, \frac{1}{2})$, i.e., $u(O+x) = -u(O-x)$. The temperature was chosen to be 1.025 at the left half, which indicated the lower density, 0.975 at the right half, which indicated the higher density:

$$\theta(x,y,t=0) = \begin{cases} 1.025\,, & \text{if} \quad x<4\,, \\ 0.975\,, & \text{if} \quad x>4\,. \end{cases} \tag{4.4}$$

By Boussinesq assumption, the density difference can be converted into temperature difference with the reverse ratio. In addition, the whole flow was at rest at $t = 0$:

$$u(x,y,t=0) = 0\,. \tag{4.5}$$

The Reynolds number is chosen to be $Re = 15,811.38$, the Prandtl number is chosen to be 1, and the Richardson number Ri, which corresponds to the gravity effect, is chosen to be 4. Before move to the numerical results, let's make a remark to explain that $u(x,y)$, the solution of equations (4.1)-(4.5), is anti-symmetric about $O(4, \frac{1}{2})$.

REMARK 4.1. *In this discussion, we let*

1. *g be the negative identity linear transform on $\mathbb{R}^2$, i.e.*

$$g\cdot(x,y) = -(x,y), \quad \textit{for} \quad (x,y)\in\mathbb{R}^2,$$

2. *$v(x,y) = u(x+4, y+\frac{1}{2})$, and*

3. *$\phi(x,y) = \theta(x+4, y+\frac{1}{2}) - 1$.*

Then equations (4.1)-(4.5) can be rewritten as

$$\begin{cases} \partial_t v + (v\cdot\nabla)v + \nabla p - Ri\cdot\begin{pmatrix} 0 \\ 1 \end{pmatrix} = \dfrac{1}{Re}\Delta v + Ri\cdot\phi\cdot\begin{pmatrix} 0 \\ 1 \end{pmatrix} \\ \partial_t\phi + (u\cdot\nabla)\phi = \dfrac{1}{Re\cdot Pr}\Delta\phi\,, \\ \nabla\cdot v = 0\,, \end{cases} \tag{4.6}$$

supplemented with the boundary and initial conditions

$$v|_{\partial\Omega_1} = 0\,, \tag{4.7}$$

$$\frac{\partial\phi}{\partial n}\Big|_{\partial\Omega_1} = 0\,, \tag{4.8}$$

$$\phi(x,y,t=0)=\begin{cases} 0.025\,, & \text{if} \quad x<0\,,\\ -0.025\,, & \text{if} \quad x>0\,, \end{cases} \tag{4.9}$$

and

$$v(x,y,t=0)=0\,, \tag{4.10}$$

where $\Omega_1=[-4,4]\times[-\frac{1}{2},\frac{1}{2}]$. *To prove that* $u(x,y)$, *the solution of problem (4.1)-(4.5), is anti-symmetric about* $O(4,\frac{1}{2})$ *is equivalent to showing v(x,y), the solution of problem (4.6)-(4.10) is anti-symmetric about* $(0,0)$. *Since conditions (4.7)-(4.10) is anti-symmetric about (0,0), it is easy to check that (4.6) is invariant under g in the sense that if* $(v,\phi)(x,y)$ *is a solution of (4.6)-(4.10) then* $g\cdot(v,\phi)(g\cdot(x,y))$ *is also a solution of (4.6)-(4.10). Hence* $(v,\phi)(x,y)=g\cdot(v,\phi)(g\cdot(x,y))$, *which means that* $v(x,y)$ *is anti-symmetric about* $(0,0)$.

A fourth order finite difference method proposed by J.-G. Liu, C. Wang and H. Johnston [9] is used in the numerical simulation of the above physical process. The numerical method employs the vorticity-stream function formulation of (4.1)-(4.3). A compact scheme is applied to the momentum equation, while the temperature transport equation is approximated by fourth order long-stencil differences, along with a one-sided extrapolation near the physical boundary. Such an extrapolation is proven to be stable and a full fourth order convergence analysis of the overall numerical scheme is established in [20]. The advantage of the scheme is that at each Runge-Kutta time stage, only two Poisson solvers are required to achieve a fourth order spatial accuracy. No-slip boundary condition is expressed by the vorticity boundary condition. Both the vorticity boundary condition and the one-sided extrapolation for the temperature around the boundary are explicitly enforced. That makes the computation very efficient.

Fig. 4.1 shows the numerical results of temperature on the resolution of 2049×257, at a sequence of time: $t_1=4.743416$, $t_2=7.115124$, $t_3=8.696264$, $t_4=10.277402$, $t_5=14.230249$, $t_6=17.392527$, respectively.

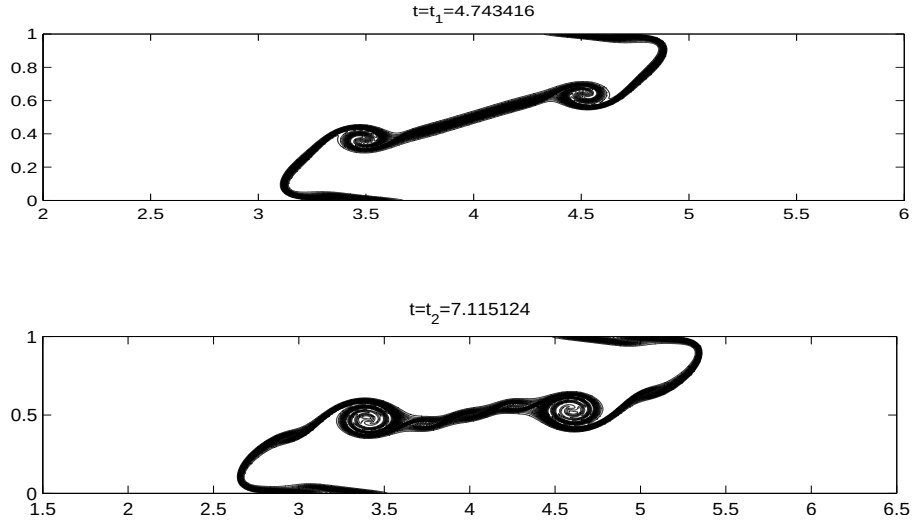

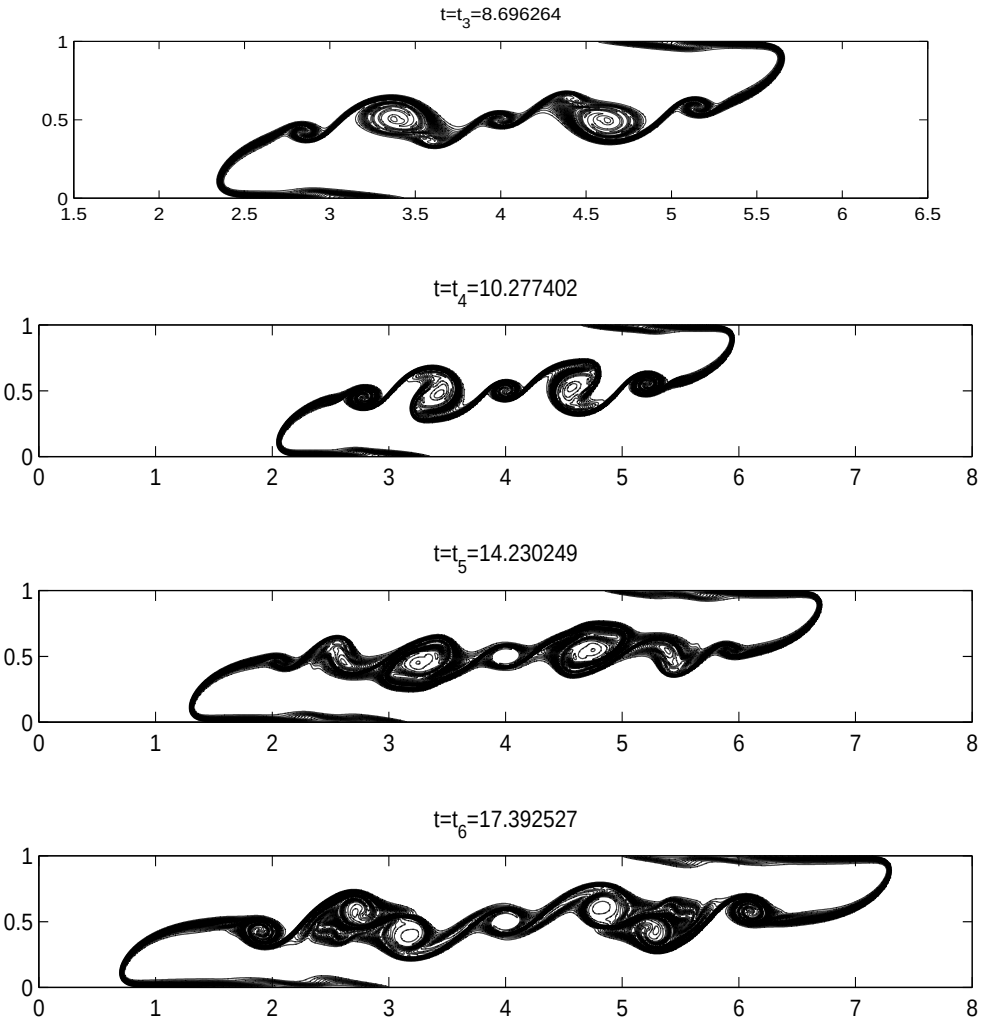

FIG. 4.1. *Contour plots of the temperature at a sequence of time.*

It can be readily seen that at least one transition of the flow's topological structure occurs between each consecutive time instant. We investigate the topological structures of the flow and their stability from the beginning to a final time $t_6 = 17.392527$. To achieve this, we need to concentrate the study on the phase diagram at different time instants, which gives complete plots of circle cells, circle bands and saddle connections of the flow. The reason for the emphasis on the phase diagram is because it illustrates the possibilities of the onset of the structural bifurcation of a divergence-free vector field with anti-symmetry characterized by Theorem 2.6.

The numerical result shows that ten structural bifurcations are presented during the whole time period (from $t = 0$ to $t = t_6 = 17.392527$). The topological structure of the flow are stable at all the time, except for ten critical time instants. These critical time instants are $T_1^* = 4.165985$, $T_2^* = 5.794874$, $T_3^* = 6.769172$, $T_4^* = 7.601483$, $T_5^* = 7.746632$, $T_6^* = 9.102300$, $T_7^* = 11.123627$, $T_8^* = 12.358814$, $T_9^* = 12.649111$ and $T_{10}^* = 15.921119$.

Eight of the transitions (at the time instants) are caused by an appearance of an interior degenerate singular point so that the first condition of stability criterion in Theorem 2.6 is violated. These cases are classified by Theorem 3.1. Namely, the appearance of an isolated degenerate singular point satisfying Assumption (H) is assured to result in a structural bifurcation. Spin off or disappearance of a center (bubble) represents a physical phenomenon corresponding structural transition. In this numerical experiment, the spin off of a bubble occurs at the time instants T_1^*, T_2^*, T_4^*, T_7^*, T_9^* and T_{10}^*; while the disappearance of a bubble occurs at the time instants T_5^* and T_8^*.

The other two transitions (at the time instants T_3^* and T_6^*) are caused by saddle connections between non-symmetric saddle points so that the second condition in Theorem 2.6 is violated. As a result, the only change in the topological structure of the flow is the style of saddle connection. These two cases do not belong to the classification of Theorem 3.1. In addition, we observe that any saddle connection between symmetric ones is stable during the time history. This provides a strong numerical evidence of the additional stability for a symmetric flow, as indicated by Theorem 2.6.

To avoid the repetitions, we focus on the mechanism of first, third and fifth structural transitions, which stand for spinning off of a bubble, saddle connection between non-symmetric ones and disappearance of a bubble, respectively. The other transitions have the same mechanism as these three examples.

4.1. The first structural bifurcation: a spin off of a bubble. A detailed numerical calculation shows that the first structural bifurcation occurs at $t = T_1^* = 4.165985$. The flow starts from the rest and forms a single center, due to the density difference and gravity force. This trivial structure persists until the first critical time. After the critical time, one center and two symmetric saddle points are presented in the velocity vector field. The corresponding phase diagrams at the three time instants $t = 3.952847$ (before the bifurcation), $t = T_1^*$ (the critical time) and $t = 4.743416$ (after the bifurcation) are given in Fig. 4.2. Different topological structures are clearly observed in the figure.

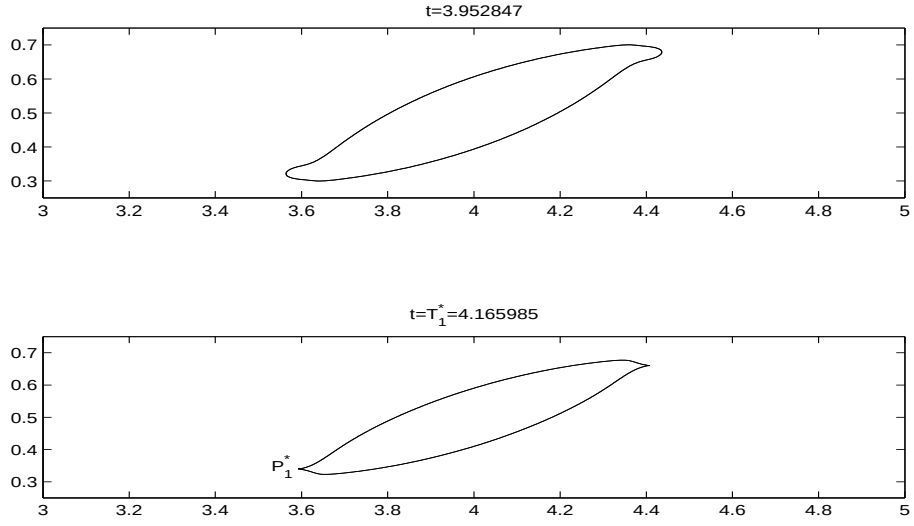

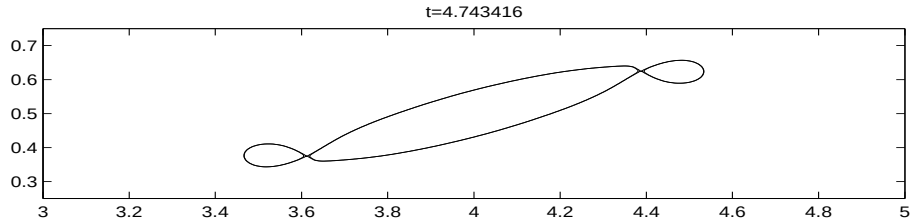

FIG. 4.2. *Phase diagrams at* $t = 3.952847, T_1^* = 4.165985, 4.743416$.

The structure at $t = 3.952847$ is stable, since it satisfies all three conditions in Theorem 2.6. In fact, the numerical evidence shows its structural stability until the first critical time T_1^*.

The structure at $t = 4.743416$ is also stable, by the classification theorem, since there is no degenerate singular point, and saddle connection only occurs between two symmetric saddles. Such a stability is also verified numerically. This structure persists until the next critical time.

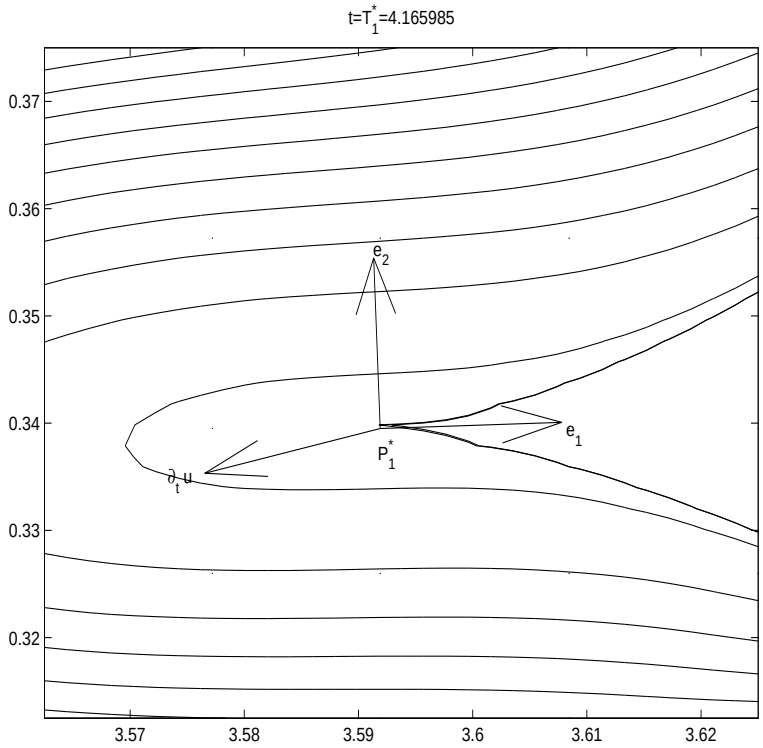

FIG. 4.3. *Zoom plot for the stream function at the first critical time* $T_1^* = 4.165985$.

However, the structure of the flow at the critical time $t = T_1^*$ is unstable. A degenerate singular point is formed at $P_1^* = (3.5917, 0.3395)$, i.e., $u(P_1^*, T_1^*) = 0$, $\det(Du)(P_1^*, T_1^*) = 0$, indicating the instability of its topological structure. Moreover, the numerical result shows that the Jacobian matrix Du is non-zero. There are two orbits connected to P_1^*, which in turn verifies that $\text{ind}(u, P_1^*) = 0$, and the

angle between the two orbits is zero. Such a result is observed in Fig. 4.3, which shows the zoom plot of the stream function near the critical point P_1^* at $t = T_1^*$. In addition, the eigenvector e_1 of the Jacobian matrix Du, the orthogonal vector e_2 and the acceleration vector $\partial_t u$ are presented in the figure. It is observed that the vector $\partial_t u$ is not orthogonal to e_2, i.e., $\partial_t u \cdot e_2 \neq 0$. As a result, Assumption (H) (given in Section 3) is satisfied. By Theorem 3.1, an interior structural bifurcation is assured to occur and the detailed process is shown in Fig 4.2.

Then we conclude that, the flow structures are stable before and after the bifurcation time, (e.g., $t = 3.952847, 4.743416$, respectively), and the only instability occurs at the critical time T_1^*. After the critical time, the flow structure at $t < T_1^*$ is bifurcated into a new structure at $t > T_1^*$. This numerical result agrees with the description outlined in Theorem 3.1.

4.2. The third structural bifurcation: instability caused by saddle connection between non-symmetric ones. The third structural bifurcation occurs at the critical time $t = T_3^* = 6.769172$. The corresponding phase diagrams at the three time instants $t = 6.324555$ (before the bifurcation), $t = T_3^*$ (the critical time) and $t = 7.115125$ (after the bifurcation) are given in Fig. 4.4.

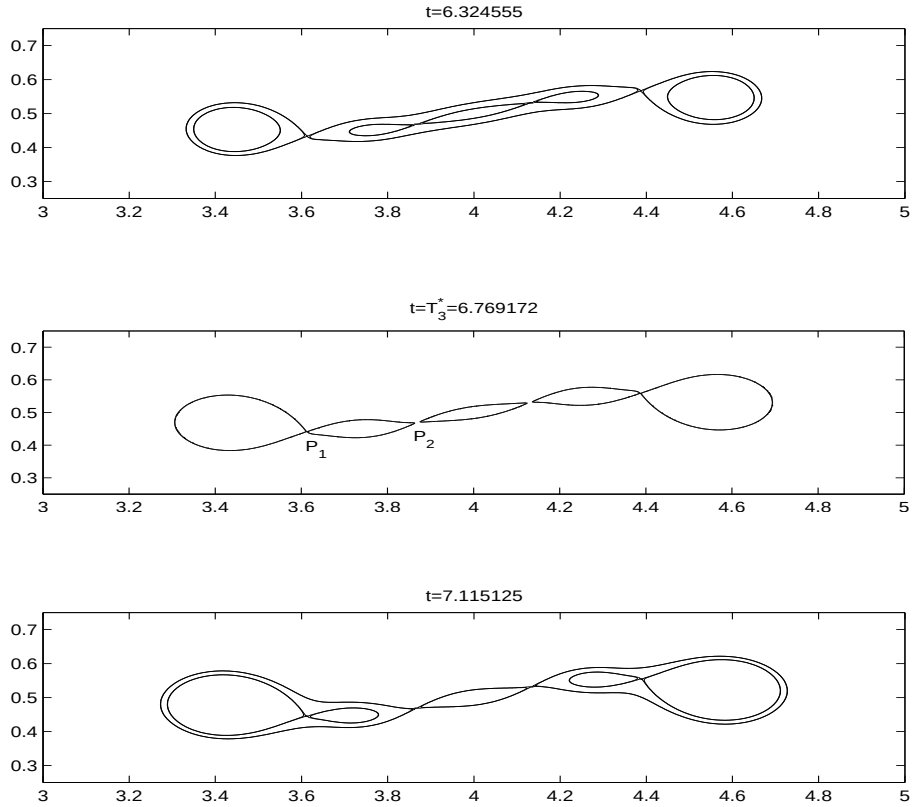

FIG. 4.4. *Phase diagrams at* $t = 6.324555, T_3^* = 6.769172, 7.115125$.

The structure of two symmetric saddle connections, after the previous bifurcation, persists at $t = 6.324555$. At $t = 7.115125$, there is one saddle connection between symmetric ones on the outer orbit. Meanwhile, there are two (symmetric) self-connected

saddles within the two tails. Similarly, the flow structures are stable at both time instants. The stability of both structures is verified by Theorem 2.6, since an interior saddle is either connected to its symmetric image or self-connected. The numerical evidence also supports such a stability.

However, the mechanism of this bifurcation is different from the first and second ones. At the critical time $t = T_3^*$, all the four saddle points are connected. In particular, an interior saddle P_1 is connected to another saddle P_2 which is not its symmetric image. This violates the second condition in the stability classification in Theorem 2.6, thus the flow structure at $t = T_3^*$ turns unstable. Yet, it can be observed that there is no generation or disappearance of a center in the flow through this bifurcation. The only difference between the flow structures before and after the critical time, each of which is stable, is the style of saddle connection. Since the cause of the instability of the flow at the critical time is not due to an appearance of a degenerate singular point, but a saddle connection between non-symmetric ones, the third bifurcation is not classified by Theorem 3.1.

4.3. The fifth structural bifurcation: a disappearance of a bubble. The fifth structural transition occurs at $t = T_5^* = 7.746632$. The corresponding phase diagrams at the three time instants $t = 7.708052$ (before the bifurcation), $t = T_5^*$ (the critical time) and $t = 7.905694$ (after the bifurcation) are given in Fig. 4.5. The difference between the structures is obvious: two symmetric centers (bubble) disappear inside an inner orbit at $t = 7.905694$.

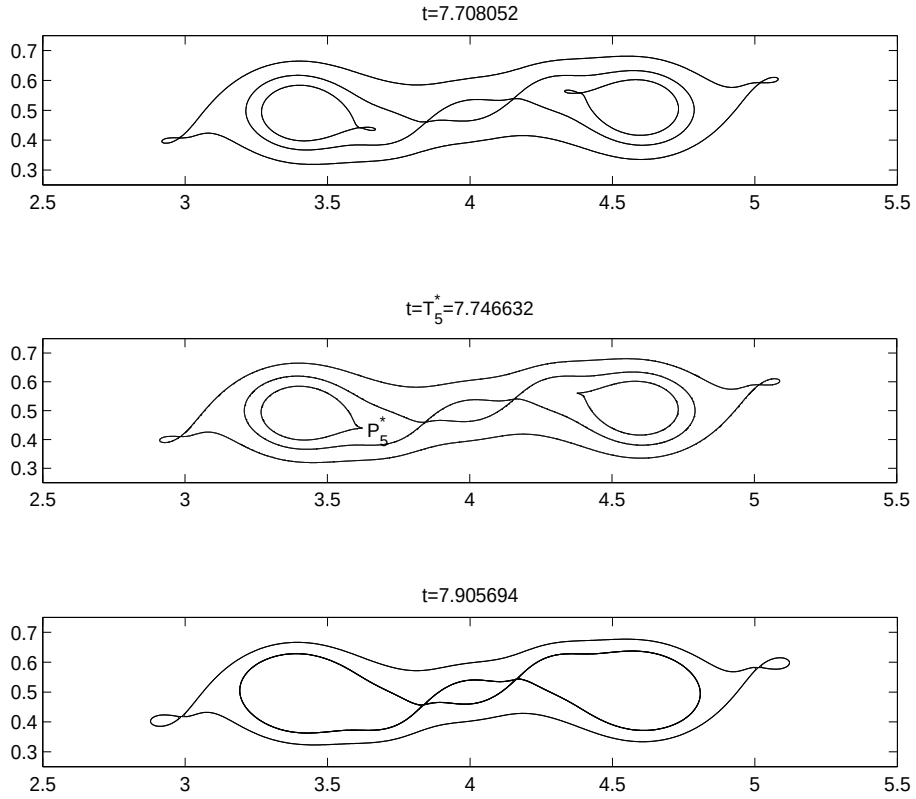

FIG. 4.5. *Phase diagrams at* $t = 7.708052, T_5^* = 7.746632, 7.905694$.

The same as the previous ones, the stability of the flow structures before and after the critical time is assured by Theorem 2.6, since a saddle connection only occurs between symmetric ones. The two structures are different, and the only instability during this time period occurs at the critical time T_5^*. The zoom plot of the stream function near the critical point P_5^* at $t = T_5^*$ is presented in Fig. 4.5.

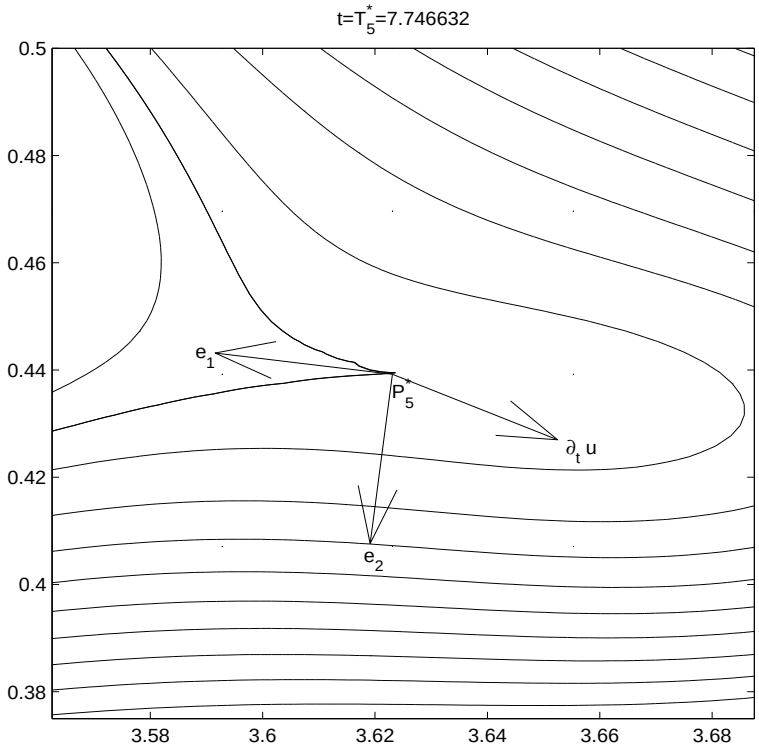

FIG. 4.6. *Zoom plot for the stream function at the fifth critical time* $T_5^* = 7.746632$.

5. Concluding remark. The structural stability and bifurcation of 2-D divergence-free vector fields with the anti-symmetry are studied in this paper. It is proven that a saddle connection between symmetric images is stable for such a anti-symmetric flow. The anti-symmetry may come from the boundary condition, initial data and the force. This addition stability due to the anti-symmetry appears in many physical situations. As an example, we simulate a simplified model of Marsigli oceanic flow at a Reynolds number $Re = 15,811.38$ and systematically study this peculiar stability property. The numerical results also reveal the detailed process of ten structural bifurcations. Spinning off of a bubble or disappearance of a bubble are caused by a degenerate singular point along with the condition (3.4), as outlined in Theorem 3.1. A connection between non-symmetric saddles also leads to an instability of the flow and therefore a structural bifurcation. For all the structural bifurcations, the numerical evidence shows that the flow keeps stable for a while except for the ten critical time instants. Our numerical experiment illustrates the mechanism of the structural bifurcations classified by Theorem 3.1 and Theorem 2.6 in a satisfactory detail.

Acknowledgement. The authors would like to thank Shouhong Wang, Tian Ma and Michael Ghil for their valuable suggestions. C. Hsia was partially supported by NSC grant 97-2115-M-002-017 and the Golden Jade Fellowship of Kenda Foundation. J.-G. Liu was partially supported by NSF grant DMS 08-11177.

REFERENCES

[1] D. Anosov and V. Arnold, *Dynamical Systems I*, Springer, New York, 1985.
[2] V. Arnold, *Mathematical Methods of Classical Mechanics*, Springer, New York, 1978.
[3] B. Cantwell, *On the behavior of velocity gradient tensor invariants in direct numerical simulations of turbulence*, Phys. of Fluids A, 5 (1993), pp. 2008–2013.
[4] M. Ghil, J.-G. Liu, C. Wang, and S. Wang, *Boundary-layer separation and adverse pressure gradient for 2-D viscous incompressible flow*, Physica D, (2004), pp. 149–173.
[5] M. Ghil, T. Ma, and S. Wang, *Structural bifurcation of 2-D incompressible flows*, Indiana Univ. Math. J., 50 (2001), pp. 159–180. Dedicated to Professors Ciprian Foias and Roger Temam (Bloomington, IN, 2000).
[6] ———, *Structural bifurcation of 2-D nondivergent flows with dirichlet boundary conditions: applications to boundary-layer separation*, SIAM J. Appl. Math., (2005), pp. 1576–1596.
[7] A. Gill, *Atmosphere-Ocean Dynamics*, Academic Press, 1986.
[8] R. Krasny and M. Nitsche, *The onset of chaos in vortex sheet flow*, J. Fluid Mech., 454 (2002), pp. 47–69.
[9] J.-G. Liu, C. Wang, and H. Johnston, *A fourth order scheme for incompressible boussinesq equations*, J. Sci. Comp., 18 (2003), pp. 253–285.
[10] T. Ma and S. Wang, *Structure of 2D incompressible flows with the Dirichlet boundary conditions*, Discrete Contin. Dyn. Syst. Ser. B, 1 (2001), pp. 29–41.
[11] ———, *Structural classification and stability of divergence-free vector fields*, Phys. D, 171 (2002), pp. 107–126.
[12] ———, *Interior structural bifurcation and separation of 2D incompressible flows*, J. Math. Phys., 45 (2004), pp. 1762–1776.
[13] ———, *Geometric Theory of Incompressible Flows with Applications to Fluid Dynamics*, Mathematical Surveys and Monographs, American Mathematical Society, 2005.
[14] J. Moser, *Stable and random motions in dynamical systems*, Princeton University Press, Princeton, N. J., 1973. With special emphasis on celestial mechanics, Hermann Weyl Lectures, the Institute for Advanced Study, Princeton, N. J, Annals of Mathematics Studies, No. 77.
[15] J. Palis, Jr. and W. de Melo, *Geometric theory of dynamical systems*, Springer-Verlag, New York, 1982. An introduction, Translated from the Portuguese by A. K. Manning.
[16] M. Peixoto, *Structural stability on two dimensional manifolds*, Topology, 1 (1962), pp. 101–120.
[17] A. Perry and M. Chong, *A description of eddying motions and flow patterns using critical point concepts*, Ann. Rev. Fluid Mech., 19 (1987), pp. 125–155.
[18] C. C. Pugh, *The closing lemma*, Amer. J. Math., 89 (1967), pp. 956–1009.
[19] C. Robinson, *Generic properties of conservative systems, part 1 and 2*, Am. J. Math., 92 (1970), pp. 562–603, 897–906.
[20] C. Wang, J.-G. Liu, and H. Johnston, *Analysis of a fourth order finite difference method for incompressible boussinesq equations*, Numer. Math., 97 (2004), pp. 555–594.